Stabilization of ZnO polar plane with charged surface nanodefects

Ju Hong Lai,[1] Shu Hsuan Su,[1] Hsin-Hsien Chen,[1] J. C. A. Huang,[1,2,*] and Chung-Lin Wu[1,†]
[1]*Department of Physics, National Cheng Kung University, Tainan, Taiwan 701, Taiwan*
[2]*Advanced Optoelectronic Technology Center, National Cheng Kung University, Tainan, Taiwan 701, Taiwan*
(Received 9 April 2010; revised manuscript received 18 August 2010)

Based on *in situ* scanning probe microscopy/spectroscopy, this study investigates the stabilization of Zn-terminated ZnO polar plane using surface defects. O-terminated surface defects on a nanometer scale, which have two morphologies, i.e., hexagonal cavities and small pits, are observed at the submonolayer depth on the (0001)-Zn surface by applying medium-energy Ar^+ bombardment (2.5 keV) at a high temperature (850 °C). Experimental results indicate that the local electronic structure of O-terminated surface defects exhibits upward band bending with respect to the Zn-terminated surface, which is consistent with the observations made using Kevin probe microscopy, in which the ZnO polar surface has a locally reversed electrostatic field. Moreover, pair-distribution analysis indicates that the O-terminated surface defects with diameters below 0.9 nm are charged with one electron per pit, thus helping to compensate for the internal polarization.

DOI: XXXX PACS number(s): 68.35.B−, 68.37.Ef, 68.47.Gh, 73.20.At

I. INTRODUCTION

Wurtzite-type zinc oxide (ZnO) has been thoroughly investigated owing to its remarkable properties, including a direct wide band gap, large exciton binding energy, excellent transparent conductivity, and catalytic effectiveness.[1] The polar surfaces of ZnO crystal are highly promising templates for use in catalysis and gas sensors owing to the excellent surface/interface properties. Thus, understanding the structural and electronic properties of the ZnO polar surface/interface is important to elucidating and operating ZnO-based devices.

In a simple ionic model,[2,3] alternately stacked Zn and O ionic layers along the *c* axis induce a macroscopic dipole field inside the ZnO crystal. Perfectly cleaved polar surfaces, (0001)-Zn and $(000\bar{1})$-O surfaces, are not naturally stable since the internal dipole field causes divergence of the electrostatic energy. Previous investigations have demonstrated that the adsorption of oppositely oriented dipole molecules[4] or metallic surface states can cancel out the electrostatic energy divergence owing to the screening effect of free charges.[5,6] However, the proposed metallic states have not been identified experimentally. Modifying surface stoichiometry by reconstruction is an alternative means of compensating for the internal dipole field. Previous scanning tunneling microscopy (STM) and atomic force microscopy (AFM) studies have demonstrated the formation of high density of triangular "magic" islands, which stabilize the (0001)-Zn surface.[7,8] Theoretical calculations reveal the correlation between the magic islands and stabilization of ZnO polar surfaces.[9,10] However, experimental evidence suggests that, rather than the magic islands, the lattice relaxation of the upper layers stabilizes the $(000\bar{1})$-O surface.[11] Structural defects, which adjust the surface stoichiometry effectively, are considered crucial to stabilize ZnO polar surfaces. Although the surface/interface defects and surface reconstructions play a significant role in determining the properties of ZnO-based devices,[12–15] their involvement in stabilizing the ZnO polar surfaces is poorly understood experimentally.

Based on Ar^+-ion bombardment and annealing treatment, this study investigates how surface defects affect the stabilization of ZnO polar surfaces. Surface defects created by middle-energy Ar^+ bombardment are O-terminated hexagonal cavities and pits at submonolayer depths on the Zn-terminated triangular islands. The structure, local density of states (LDOS), and surface potential of the surface defects on the (0001)-Zn surface are explored *in situ* by STM, scanning tunneling spectroscopy (STS), and Kelvin probe microscopy (KPM). According to the pair-distribution statistics of defect pits at a sublayer depth, O-terminated surface defects with negative charge can lower the electrostatic energy of (0001)-Zn polar surface.

II. EXPERIMENT

Experiments were performed in an ultrahigh-vacuum (UHV) system (JSPM-4500 A/S; JEOL Ltd.), which consisted of a sample preparation chamber and a STM/AFM observation chamber. The (0001)-Zn single crystal was purchased from Techno Chemic, Inc. A clean and atomically flat (0001)-Zn surface was obtained by sputtering the Zn-polished side of ZnO crystal through use of an Ar^+-ion beam at 1 keV with an ion current of 0.5–0.6 μA for 20 min, followed by annealing at 650 °C in UHV for 20 min using four or five sputter-annealing cycles. Surface defects were then produced in a controlled manner by bombarding the atomically flat (0001)-Zn surface again using an Ar^+-ion beam at 2.5 keV and 850 °C in 3×10^{-6} torr. Next, the surface crystallinity and cleanliness of the (0001)-Zn surface were examined *in situ* using reflection high-energy electron diffraction (RHEED) and x-ray photoelectron spectroscopy (XPS), respectively. By using UHV STM/AFM, both the clean (0001)-Zn surface and the modified surface morphology produced by subsequent ion bombardment were probed. All STS spectra were obtained using a lock-in amplifier to eliminate noise from the conductivity values (dI/dV) and the difficulty of differential, mathematical analysis. In the KPM mode, a tunable dc bias and a modulated ac voltage were applied to the sample surface and the $PtIr_3$-coated AFM tip, respectively.[16] During scanning, the electrostatic force between the sample surface and the AFM tip was minimized by

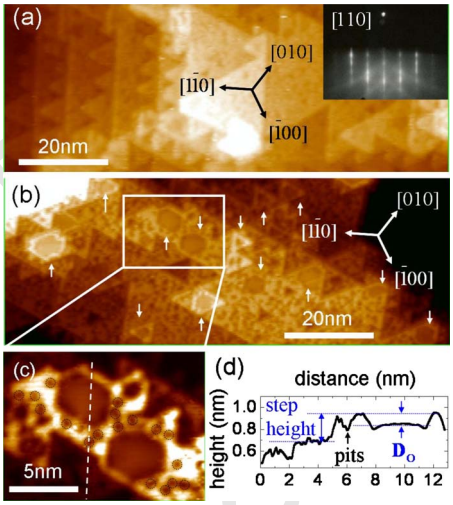

FIG. 1. (Color online) Surface morphology of (0001)-Zn surface treated by (a) initial cleaning and (b) 2.5 keV Ar^+-ion bombardment at 850 °C. Inset in (a) shows the RHEED image of (0001)-Zn surface when the e-beam is incident in the direction of [110].(c) Zoom-in STM image (15 nm × 12 nm) of (0001)-Zn surface treated by 2.5 keV Ar^+-ion bombardment at 850 °C. (d) Height profile along scanned line in (c).

tuning the sample bias. This sample bias represents the surface potential of each pixel on the KPM image.

III. RESULTS AND DISCUSSION

Surface morphology of the initially clean (0001)-Zn surface includes many characteristic triangular islands, as shown in Fig. 1(a). The triangular islands consist of a Zn-O double layer approximately 2.6 Å in height. Edge sizes of the triangular islands on the initially clean (0001)-Zn surface range from 6 to 15 nm, which correlates with the dimensions of triangular islands in previous studies.[6,7] The RHEED study revealed that the clean (0001)-Zn surface was a (1 × 1) structure without surface reconstruction [Fig. 1(a), inset]. In the following, the clean (0001)-Zn surface was further treated by 2.5 keV Ar^+ bombardment at 850 °C; in addition, hexagonal cavities with nanometer sizes appeared on the triangular islands [indicated by arrows in Fig. 1(b)]. Moreover, the ion-bombarded surface is rougher than the clean ZnO surface, revealing that such treatment can effectively produce a large number of surface defects.

To show the surface defects more clearly, Fig. 1(c) zooms in on the marked frame in Fig. 1(b). The large surface defects, including the hexagonal cavities, typically have a diameter of 4–5 nm. Interestingly, the corresponding height profile [Fig. 1(d)] reveals that the typical depth of the hexagonal cavities (D_0=1.1 ± 0.2 Å) is significantly less than the height of one Zn-O double layer (2.6 Å). Several smaller, irregular pits with a depth similar to that of the hexagonal cavities and diameters of 0.6–1.2 nm were distributed on the surface [Fig. 1(c), black dotted circles]. Moreover, the electrostatic nature of the hexagonal cavities was clarified by applying STS to determine their local electronic properties on the Zn-terminated surface.

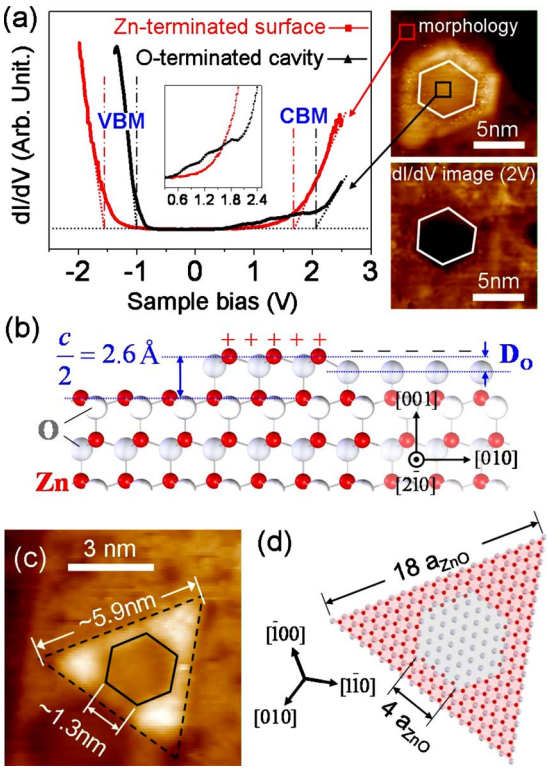

FIG. 2. (Color online) (a) STS spectra of hexagonal cavities and Zn-terminated surface. Data were obtained using a lock-in amplifier and a modulated voltage of 0.3 V. (b) Surface charge distribution in O-terminated cavity and Zn-terminated surface. (c) STM image for a single O-terminated hexagonal cavity inside Zn-terminated triangular island. (d) Schematic sketch for the top view of atomic model of (c).

Figure 2(a) reveals that the behavior of surface conductivity inside the hexagonal cavity depends on the sample bias that is proportional to LDOS ranging from the valence-band maximum (VBM) to the conduction-band minimum (CBM). The average dI/dV spectra were obtained from various positions of Zn-terminated surface and the defect surface (inside the hexagonal cavities). The dI/dV spectra of both surfaces reveal typical semiconducting behavior with a band gap of about 3.1 eV. The VBM and CBM on the surface defects exhibit upward bending of about 0.5 eV and 0.3 eV, respectively, relative to the VBM and CBM on the Zn-terminated surface, revealing the local inhomogeneity of the electrostatic field. In the dI/dV spectra of the hexagonal cavities [Fig. 2(a), inset], several intergap states can be observed from 0.8 to 1.8 V, possibly originating from the various vacancies of ZnO showing donorlike behaviors with the energy level below the CBM.[17] The surface impurity induced intergap states can be ruled out due to the XPS spectra with no impurity related peaks (not shown here). Thus, according to the depth analysis [Fig. 1(d)], the small pits can be considered Zn vacancies with O-terminated surfaces having hexagonal shapes and small pits, which were formed by desorption of surface Zn atoms under Ar^+ bombardment. The physical distance between Zn and O planes (0.69 Å) differs from that measured with STM (1.1 ± 0.2 Å), probably due to the electronic effects. Inhomogeneity of the electrostatic

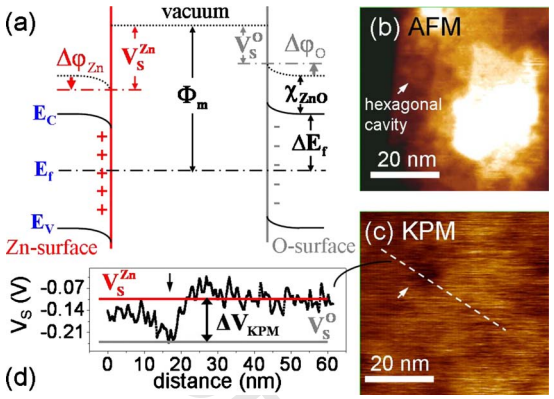

FIG. 3. (Color online) (a) Schematic energy diagram of KPM. (b) AFM image of (0001)-Zn surface treated by 2.5 keV Ar^+ bombardment. (c) KPM image corresponding to the AFM image. (d) Surface potential (V_S) height profile of scanned line in (c). The arrows in (c) and (d) indicate the position of hexagonal cavity.

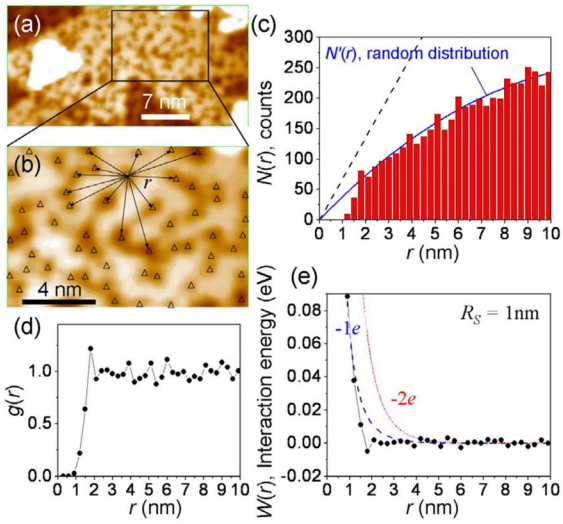

FIG. 4. (Color online) (a) STM image (35 nm × 17.5 nm) of small pits on the (0001)-Zn surface treated by 2.5 keV Ar^+ bombardment. (b) Zoomed-in image (13 nm × 8.7 nm) from the marked frame of (a). Where r denotes the separation between the reference pit and the neighboring pits. (c) Statistical distribution $N(r)$ of the pair distance r. (d) Pair-correlation function, $g(r)$. (e) Interaction energy $W(r)$ between the small pits. Fitted curve (dashed line) for interaction energy is obtained from the screened Coulomb potential $V(r)$.

field can be attributed to the O-terminated surface regions with charges that oppose the charges of the Zn-terminated surface region, as schematically displayed in Fig. 2(b).

During the Ar^+ bombardment and annealing, Zn and O atoms on the (0001)-Zn surface are highly mobile and become rearranged in a manner that compensates for the divergence of electrostatic energy. Previous studies[6,7] found the characteristic triangular islands with O-terminated step edges on the (0001)-Zn surface, explaining why the net electrostatic field at the step edges cancels out the internal dipole field. In this study, a unique morphological feature in the form of a hexagonal cavity was found on the characteristic triangular island [Fig. 2(c)]. Figure 2(d) illustrates the relationship between the lattice geometries of the O-terminated hexagonal cavity and the Zn-terminated triangular island. As is estimated, the surface stoichiometry of O/Zn is approximately 0.71, which closely corresponds to that required (0.75) to ensure the stability of the ZnO polar surfaces.[6,7,11] Therefore, modification of the stoichiometry for the stability of polar surface can be related to the redistribution of the surface charge on the (0001)-Zn surface through the formation of O-terminated defects. To confirm this claim, KPM, which is sensitive to electrostatic properties,[18,19] was applied to determine the surface potential.

The surface potential represents the difference between the work function of the sample surface and that of the metal-coated AFM tip (Φ_m). According to Fig. 3(a), the surface potential of the Zn-terminated surface (V_S^{Zn}) and the O-terminated surface region (V_S^O) can be estimated using $V_S^{Zn}=\Phi_m-\chi_{ZnO}+\Delta\varphi_{Zn}-\Delta E_f$ and $V_S^O=\Phi_m-\chi_{ZnO}-\Delta\varphi_O-\Delta E_f$, where χ_{ZnO} is the electron affinity of ZnO; ΔE_f is the energy difference between the bulk conduction band and the Fermi level, and $\Delta\varphi_{Zn}$ ($\Delta\varphi_O$) denotes the band bending caused by the surface charges on the Zn-terminated surface (associated with the hexagonal cavities and pits). Therefore, the difference between V_S^O and V_S^{Zn} (ΔV_{KPM}) equals $\Delta\varphi_{Zn}+\Delta\varphi_O$, suggesting that the difference between the surface potentials depends on the distribution and sign of the surface charge.

Figure 3(b) shows the KPM image and the corresponding AFM image of the hexagonal cavities on the Zn-terminated triangular islands. Although the AFM herein is not sufficiently sensitive to probe the small pits, the observed depths of hexagonal cavities closely correspond to the results of the STM study. The O-terminated (hexagonal cavities) and the Zn-terminated (triangular islands) surfaces are regions of relatively low (dark) and high (bright) surface potential, respectively. According to the surface potential profile of the line scan across the Zn-terminated surface and the hexagonal cavities, V_S^O is approximately 80 ± 30 mV below V_S^{Zn}, which is consistent with KPM observations in related ZnO surfaces.[18,19] This observation suggests that, as expected, the O-terminated surface defect has a negative surface charge with respect to the Zn-terminated surface. Restated, the surface defects, including the hexagonal cavities and pits, result in a locally reversed electrostatic field to cancel out the internal dipole field, subsequently reducing the electrostatic energy. To quantify the charge of the surface defects, the pair-distribution statistics, which are involved in the interaction between the charged surface defects, are characterized as follows.

Figure 4(a) shows that the small pits with diameters of 0.6–1.2 nm at the sublayered depth are distributed on the (0001)-Zn polar surface. In a many-body system of the O-terminated pits, the equilibrium distribution of the pits depends on how neighboring pits affect each pit. Finding the clustering of pits is nearly impossible, revealing that the short-ranged repulsive Coulomb interaction occurs on the distribution of pits. To verify the repulsive interaction, the statistical distribution $N(r)$ of all possible pair distances r between the pits, which was counted from all the pit positions in the STM image [as indicated by the symbol △ in Fig. 4(b)], are used [Fig. 4(c)]. In is noted that the pits are

selected from their diameters below 0.9 nm, which matches the size of a single Zn vacancy (V_{Zn}) as the equal charge of each pit in the statistics of pair distribution. By comparing with the random distribution $N'(r)$ of pair distances r in the absence of pit-pit interactions, the pair-correlation function $g(r)$ can be obtained from $g(r)=\frac{N(r)}{N'(r)}$, as shown in Fig. 4(d).[20] In a two-dimensional system, the ideal $N'(r)$ should be regarded as $2\pi r dr\langle\rho\rangle$ [as denoted by the dashed line in Fig. 4(c)], where dr and $\langle\rho\rangle$ denote the statistical interval and the average density of the pits, respectively. However, the counts of a larger r would be confined by the finite scan size of STM images. Thus, $N'(r)$ must be corrected using the geometric factor $P(r)=r[1-\frac{r(4a-4r+\pi r)}{\pi a^2}]$ [as denoted by the solid line in Fig. 4(c)], where a is the scan size of square-shaped STM images.[21] According to the statistical approach of the mean force potential, i.e., written as $W(r)=-kT\ln[g(r)]$,[22] the interaction energy $W(r)$ between the pits on the surface at room temperature ($T=300$ K) can be determined [Fig. 4(e)]. The decay of $W(r)$ between 1 and 2 nm refers to a situation in which the effective range of the repulsive interaction can be determined by about 1.8 nm as $W(r)$ reduces to zero. Additionally, from the STM images [for example, Fig. 4(b)], the average separation between the pits and their neighboring pits can be estimated as about 2.5 nm. While the effective range of the interaction is smaller than the average separation, the correlation effects can be neglected, facilitating a description of the many-body system as a screened Coulomb potential surrounding each pit with an equal charge q.[23,24] Therefore, the screened Coulomb potential $V(r)=\frac{q}{4\pi\varepsilon_0\varepsilon}\cdot\frac{1}{r}\cdot\exp(\frac{-r}{R_S})$ can be applied to fit $W(r)$, where R_S and ε represent the screening length and the dielectric constant of ZnO (8.5), respectively.[23–25] Theory of electrostatics indicates that the screening length R_S depends only on the concentration of charge carriers (n) and ε.[24] Notably, solving the screened Poisson equation in a system of free charge carriers at room temperature ($T=300$ K) allows us to estimate the value of R_S at ~ 1.0 nm according to the solution of $R_S=\sqrt{\frac{2\pi^2\varepsilon_0\varepsilon\hbar^3}{e^2(m_e^*)^{3/2}(2\pi kT)^{1/2}F_{-1/2}(\eta)}}$, where $F_{-1/2}(\eta)$ is the Fermi-Dirac integral as a function of the reduced Fermi energy $\eta=\frac{E_F-E_C}{kT}$, depending on the concentration of charge carriers of ZnO (herein, $n\sim 6\times 10^{19}$ cm^{-3}).[22,24,26] To determine the fitting of $W(r)$ with $V(r)$, all possibilities of q that are related to the charge of V_{Zn}: $-1e$ or $-2e$ must be considered,[17,27] as shown in Fig. 4(e). The best fitting [Fig. 4(e), dashed line] indicates that the repulsive interaction on each pit with q of about $1e$ is screened by the neighboring charge carriers at R_S of 1.0 nm. This finding implies that each pit (<0.9 nm) can be regarded as a single V_{Zn} with the charge state of $-1e$, which can involve the configuration of the dangling bonds within V_{Zn}.[27] However, the charge of the larger pits (their diameters >0.9 nm), which consist of several V_{Zn}, should be larger than $1e$ owing to the increase in dangling bonds within the configuration of the pits. For dangling bonds on the O-terminated defects that do not exhibit a reconstruction, their negative charge should be enhanced with increasing the size of the surface defects.

Moreover, a weak attraction (−0.01 eV) exists at $r=2$ nm. The energy of the attractive interaction may be caused by the many-body effects when the concentration of charged pits is high ($>10^{20}$ cm^{-3}).[22,25] Because the range of interaction dominates the distribution of charged pits, R_S can be considered a physical limit for the concentration of the charged pits on the (0001)-Zn surface.[22] In the simulation based on the many-body effects for $R_S=1.0$ nm,[25] the attractive interaction between the pits also occurs at $r\sim 2$ nm, and the concentration of charged pits is determined to be approximately 1.5×10^{20} cm^{-3} which is close to the concentration of the pits (3.2×10^{20} cm^{-3}) in the STM images. The concentration of the pits is derived from the surface density (8.3×10^{12} cm^{-2}) per the layer spacing ($c/2$). According to the approximate charge of each pit ($1e$), the pits-induced surface polarization can be determined as about 1.33 $\times 10^{-2}$ C/m^2, which correlates well with the theoretical value of spontaneous polarization of ZnO (5.2 $\times 10^{-2}$ C/m^2).[28] Therefore, in combination with the increasing charge of the larger surface defects, the formation of surface defects should produce a sufficient negative charge to compensate for the internal polarization of ZnO to stabilize the surface energy. Although the statistical analysis in classical electrostatics cannot describe the system of charged surface defects accurately, this approach can provide an intuitive and comprehensive means of quantifying the redistribution of surface charge.

IV. CONCLUSION

This study investigates the origin of surface defects on stabilization of polar surface. Ar^+ bombardment at a moderate kinetic energy effectively produced the surface defects of hexagonal cavities and small pits on the (0001)-Zn polar surface, both with a submonolayer depth. According to STS and KPM investigations, surface defects with negative charges on the (0001)-Zn polar surface exhibit local reversals of the electrostatic field. Additionally, the O-terminated surface pits with negative charges, undergoing electrostatic interactions, modify the surface stoichiometry in a manner of the redistribution of surface charge for reducing of the electrostatic energy of the polar surface.

ACKNOWLEDGMENTS

The authors would like to thank the National Science Council of the Republic of China, Taiwan and the Center for Micro-Nano Technology at National Cheng Kung University, Taiwan for financially supporting this research.

*jcahuang@mail.ncku.edu.tw
†clwuphys@mail.ncku.edu.tw

[1] S. J. Pearton, D. P. Norton, K. Ip, Y. W. Heo, and T. Steiner, Prog. Mater. Sci. **50**, 293 (2005).
[2] P. W. Tasker, J. Phys. C **12**, 4977 (1979).
[3] C. Noguera, J. Phys.: Condens. Matter **12**, R367 (2000).
[4] A. Wander and N. M. Harrison, J. Chem. Phys. **115**, 2312 (2001).
[5] A. Wander, F. Schedin, P. Steadman, A. Norris, R. McGrath, T. S. Turner, G. Thornton, and N. M. Harrison, Phys. Rev. Lett. **86**, 3811 (2001).
[6] B. Meyer and D. Marx, Phys. Rev. B **67**, 035403 (2003).
[7] O. Dulub, U. Diebold, and G. Kresse, Phys. Rev. Lett. **90**, 016102 (2003).
[8] F. Ostendorf, S. Torbrügge and M. Reichling, Phys. Rev. B **77**, 041405(R) (2008).
[9] G. Kresse, O. Dulub, and U. Diebold, Phys. Rev. B **68**, 245409 (2003).
[10] M.-H. Du, S. B. Zhang, J. E. Northrup, and S. C. Erwin, Phys. Rev. B **78**, 155424 (2008).
[11] N. Jedrecy, M. Sauvage-Simkin, and R. Pinchaux, Appl. Surf. Sci. **162-163**, 69 (2000).
[12] K. A. Alim, V. A. Fonoberov, and A. A. Balandin, Appl. Phys. Lett. **86**, 053103 (2005).
[13] B. Lin, Z. Fu, and Y. Jia, Appl. Phys. Lett. **79**, 943 (2001).
[14] S. B. Zhang, S.-H. Wei, and A. Zunger, Phys. Rev. B **63**, 075205 (2001).
[15] D. C. Look, Mater. Sci. Eng., B **80**, 383 (2001).
[16] S. Kitamura and M. Iwatsuki, Appl. Phys. Lett. **72**, 3154 (1998).
[17] F. Oba, A. Togo, I. Tanaka, J. Paier, and G. Kresse, Phys. Rev. B **77**, 245202 (2008).
[18] E. Palacios-Lidón, B. Pérez-García, P. Vennéguès, J. Colchero, V. Muñoz-Sanjosé, and J. Zúñiga-Pérez, Nanotechnology **20**, 065701 (2009), the author's supporting information.
[19] J. Zúñiga-Pérez, V. Muñoz-Sanjosé, E. Palacios-Lidón, and J. Colchero, Phys. Rev. Lett. **95**, 226105 (2005).
[20] K.-J. Chao, C.-K. Shih, D. W. Gotthold, and B. G. Streetman, Phys. Rev. Lett. **79**, 4822 (1997).
[21] J. Repp, F. Moresco, G. Meyer, K.-H. Rieder, P. Hyldgaard, and M. Persson, Phys. Rev. Lett. **85**, 2981 (2000).
[22] T. L. Hill, *Statistic Mechanics* (McGraw-Hill, New York, 1956).
[23] Ph. Ebert, X. Chen, M. Heinrich, M. Simon, K. Urban, and M. G. Lagally, Phys. Rev. Lett. **76**, 2089 (1996).
[24] R. B. Dingle, Philos. Mag. **46**, 831 (1955).
[25] Ph. Ebert, T. Zhang, F. Kluge, M. Simon, Z. Zhang, and K. Urban, Phys. Rev. Lett. **83**, 757 (1999).
[26] D. A. Neamen, *An Introduction to Semiconductor Devices* (McGraw-Hill, New York, 2005).
[27] P. Erhart, K. Albe, and A. Klein, Phys. Rev. B **73**, 205203 (2006).
[28] A. Dal Corso, M. Posternak, R. Resta, and A. Baldereschi, Phys. Rev. B **50**, 10715 (1994).